Diabetes, Metabolic Syndrome and Obesity

Dovepress
Taylor & Francis Group

Open Access Full Text Article

ORIGINAL RESEARCH

Targeting AGE-RAGE Signaling Pathway with Hujin Decoction Ameliorates MAFLD in HepG2 Cells

Zixuan Zhang[1,*], Jiaxi Shi[2,*], Fuxuan Liu[1], Jing Zhou[1], Qi Shen[3], Xuguang Shi[1]

[1]School of Pharmaceutical Sciences, Guangzhou University of Chinese Medicine, Guangzhou, 510006, People's Republic of China; [2]The First School of Clinical Medicine, Guangzhou University of Chinese Medicine, Guangzhou, 510405, People's Republic of China; [3]Science and Technology Innovation Center, Guangzhou University of Chinese Medicine, Guangzhou, 510405, People's Republic of China

*These authors contributed equally to this work

Correspondence: Xuguang Shi, School of Pharmaceutical Sciences, Guangzhou University of Chinese Medicine, Guangzhou, People's Republic of China, Tel +8613602740975, Email sxg6902@126.com

Purpose: To explore the mechanism and substance basis of HJD for the treatment of MAFLD based on system pharmacology.

Patients and Methods: The ingredients of HJD in vitro and in vivo were detected by UPLC-MS/MS, then network pharmacology and molecular docking technology were used to predict the mechanism and substance basis, then the establishment of in vitro MAFLD model was confirmed by oil red O staining and ELISA technology, and finally the mechanism was verified by PCR, WB and flow cell technology.

Results: System pharmacology determined that succinic acid, Ginsenoside Rh4, Caffeic acid, 7-Methoxycoumarin, 5-Acetylsalicylic acid and other ingredients were the basis of pharmacodynamic substances, while RAGE[Advanced glycosylation end product-specific receptor (RAGE)], BCL2[Apoptosis regulator Bcl-2 (BCL2)], and CASP3[Caspase-3 (CASP3)] were predicted as the core targets, and AGE-RAGE was the key pathway. In vitro experiments confirmed that HJD can reduce hepatocyte apoptosis by downregulating the AGE-RAGE signaling pathway to alleviate MAFLD.

Conclusion: HJD may act on RAGE, BCL2, CASP3, and other key targets to regulate the AGE-RAGE signaling pathway through succinic acid, Ginsenoside Rh4 and Caffeic acid. This study provides a theoretical basis for the clinical application and quality control of HJD.

Keywords: Hujin decoction, MAFLD, UPLC-MS/MS, molecular docking, network pharmacology, AGE-RAGE pathway

Introduction

MAFLD is a condition of hepatic fat accumulation combined with metabolic dysfunction in the form of overweight or obesity and insulin resistance. It is also associated with an increased risk of cardiovascular diseases, including hypertension and atherosclerosis.[1] Currently, MAFLD affects one in four people in the world.[2] It is the major cause of liver cirrhosis and hepatocellular carcinoma,[3,4] which is also expected to be the most common indication for liver transplantation by 2030.[5]

In the pathogenesis of MAFLD, the most representative theory is the "second hit" theory, in which insulin resistance occupies the central position. However, with the deepening of research and the accumulation of discoveries, this theory has gradually expanded into a more comprehensive "multiple parallel hits"[6] This new theory highlights the key role of factors such as fat accumulation, oxidative stress, ER stress, and lipotoxicity in the development of MAFLD.[7,8] In clinical studies, common MAFLD treatments include the regulation of blood glucose and lipid metabolism to provide liver protection and anti-inflammation.[9] However, the therapeutic effect is not very thorough because its pathogenesis has not been fully elucidated.[10] Given the harmfulness of MAFLD, there is an urgent need to deeply explore its pathogenesis, identify new therapeutic targets, and develop effective therapies.

The HJD has been the clinical experience of Professor Huang Zhaosheng for many years. It has been used in the treatment of MAFLD for more than 20 years and consists of six traditional Chinese medicines, namely, *Polygonum*

Received: 2 December 2024
Accepted: 22 April 2025
Published: 29 May 2025

cuspidatum Sieb.et Zucc., *Curcuma aromatica* Salisb., *Alisma plantago-aquatica* L., *Crataegus pinnatifida* Bunge, *Panax notoginseng* (Burkill) F. H. Chen ex C. H. Chow, and *Ganoderma lucidum* (Curtis) P. Karst, which have shown good therapeutic effects on MAFLD.[11–16] Previous in vivo experiments show that,[17,18] HJD can improve liver function, blood lipid levels, and lipid deposition in liver tissue in MAFLD mice by regulating the SIRT1 / AMPK / MTOR pathway. Taking advantage of the multi-ingredient, multi-target, and multi-action characteristics of traditional Chinese medicine ingredients, this study analyzed the ingredients of HJD in vitro and in vivo by UPLC-MS/MS and initially established the active ingredient library of HJD. Subsequently, the active ingredients and core targets of HJD treatment for MAFLD were identified through network pharmacology, bioinformatics technology, and molecular docking. An in vitro model of MAFLD was then established. By employing oil red O staining, ELISA, PCR, WB, and flow cytometry, we aimed to elucidate the therapeutic basis and mechanisms underlying HJD's efficacy in treating MAFLD. The study route is illustrated in Figure 1.

Materials and Methods

Experimental Animals and Cells

Twelve healthy SPF SD male rats, weighing 200–220 g, were purchased from Guangdong Weitong Lihua Laboratory Animal Technology Co., Ltd., production license number: SCXK (Guangdong) 2022–0063, qualification certificate number: No. 44829700018150. Experimental animals were raised in the SPF animal room of the School of Traditional Chinese Medicine, Guangzhou University of Chinese Medicine. The license number was SYXK (Guangdong) 2019–0202, and the feeding specifications were 6 animals per cage. The animals were fed with feed and free drinking water, and the feed and purified water were changed once a day. The room temperature was 25±1°C, the relative humidity was 40–70%, and the circadian rhythm was 12 hours (06:00 ~ 18:00). Hepg2 cells were purchased from Wuhan Pricella Biotechnology Co., Ltd.

Materials and Reagents

Polygonum cuspidatum Sieb.et Zucc., *Curcuma aromatica* Salisb., *Alisma plantago-aquatica* L., *Crataegus pinnatifida* Bunge, *Panax notoginseng* (Burkill) F. H. Chen ex C. H. Chow, and *Ganoderma lucidum* (Curtis) P. Karst. were purchased from Guangdong Kangmei Pharmaceutical Co., LTD (Puning China). BCL2, CASP3, and RAGE were purchased from Hangzhou Hua Biotechnology Co., Ltd. LTD (Hangzhou China). FFA, TC, TG, NO, and ROS ELISA kits were purchased from Jiangsu Meimian Industrial Co. Ltd. (Yancheng, China). The cell/tissue total RNA rapid

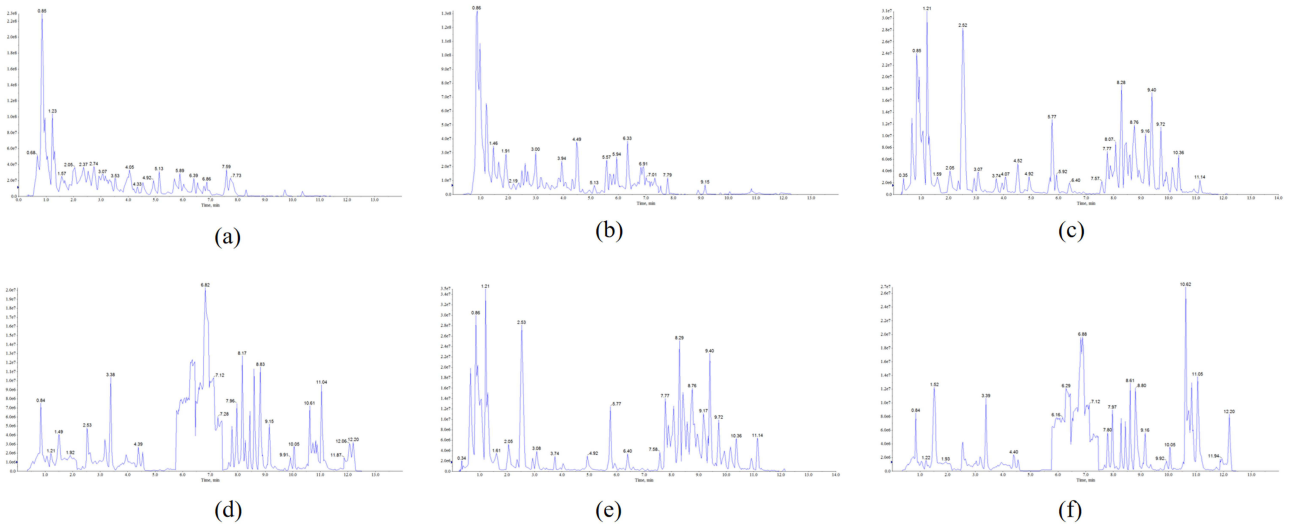

Figure 1 TIC in positive and negative ion mode. (**a**) Positive ion pattern of HJD ingredients in vitro. (**b**) Negative ion pattern of HJD ingredients in vitro. (**c**) Positive ion pattern of HJD drug-containing plasma. (**d**) Negative ion pattern of HJD drug-containing plasma. (**e**) The blank plasma positive ion pattern. (**f**) Negative ion pattern of Blank plasma.

extraction kit was purchased from New Saimei Biotechnology Co., LTD (Suzhou, China). 2x Color SYBR Green qPCR Master Mix (ROX2) was purchased from EZBioscience (California, USA); Annexin V-APC/PI Apoptosis Kit was purchased from Elabscience (California, USA), and the Oil Red O staining kit was purchased from Shanghai Bi yuntian Biotechnology Co., LTD (Shanghai, China).

Preparation of HJD

Preparation of in vitro Solution of HJD

Polygonum cuspidatum Sieb.et Zucc., *Curcuma aromatica* Salisb., *Panax notoginseng* (Burkill) F. H. Chen ex C. H. Chow, *Alisma plantago-aquatica* L., *Crataegus pinnatifida* Bunge, and *Ganoderma lucidum* (Curtis) P. Karst were weighed at a ratio of 3:3:3:2:2 and extracted twice by heating and reflux. One hour at a time. After concentration to a certain volume, the supernatant was centrifuged, filtered through a 0.22μm microporous filter membrane, and stored in a refrigerator at −20 °C for UPLC-MS/MS detection.

Preparation of the in vivo Solution of HJD

Preparation of gavage solution: Similar to the preparation of the in vitro solution of HJD. Administration method and sample processing: Twelve SD rats were randomly divided into blank and administration groups, with six rats in each group, and were adaptively fed for at least one week according to the method described in section 2.2.1. The rats in the drug administration group and the blank group were administered the same volume of distilled water and the drug solution by gavage at 7.35 g/kg (6.3 times the clinical equivalent dose in humans) once a day, respectively. After 6 consecutive days of administration, the rats was fasted for 12h (free water) before administration on day 7, and was anesthetized by intraperitoneal injection of 3% sodium pentobarbital (0.2 mL/100g) after the last lh administration. Blood was collected from the abdominal aorta and transferred into an anticoagulant vessel. After centrifugation at 3000r/min for 15 min, the supernatant was aliquots into 1.5 mL ep tubes to obtain rat blank plasma and drug-containing plasma. The samples were filtered through 0.22μm microporous filters and stored at −20 °C for UPLC-MS/MS detection.

UPLC-MS/MS Analysis Conditions and Data Processing

Chromatographic conditions: Agilent SB-C18 column (2.1 × 100 mm, 1.8 μ m), mobile phase: phase A is ultrapure water (adding 0.1% formic acid), phase B is b key (adding 0.1% formic acid), column temperature 40°C, flow rate 0.35 mL · min-1, injection volume 2 μ L. Gradient elution conditions are shown in Table 1.

The Mass spectrometry conditions were as follows: electrospray ionization (ESI) temperature, 500°C; ion spray voltage (IS), 5500 V (positive ion mode) / −4500 V (negative ion mode); ion source gas I (GSI), gas II (GSII), and air curtain gas (CUR) set to 50, 60, and 25 psi, respectively; collision-induced ionization parameters were set to high values. QQQ scans used the MRM mode and set the collision gas (nitrogen) to the medium. DP and CE of each MRM ion pair were determined by optimizing the declustering potential (DP) and collision energy (CE)ons. A specific set of MRM ion pairs was monitored during each period based on the metabolites eluted within each period. Data processing: Qualitative and quantitative analyses of the sample metabolites were performed based on the local metabolic database. Using the characteristic ion of each material, the signal intensity of the characteristic ion (CPS) in the detector, open the machine mass spectrum under the sample with MultiOuant software, integrate and correct the chromatoFigureic peak, the peak

Table 1 Gradient Conditions of ChromatoFigureic Elution

Time /min	A/%	B/%
0.00	95	5
9.00	5	95
10.00	5	95
11.00	95	5
14.00	95	5

https://doi.org/10.2147/DMSO.S506350

area of each chromatoFigurey peak (Area) represents the relative content of the corresponding material, and finally exports all chromatoFigureic peak area integral data.

Instrument calibration and performance monitoring: Instrument quality calibration (mass deviation ≤0.1 amu) and resolution verification (resolution ≤0.9 amu at 10% peak height of full width) were performed daily before analysis to ensure that the instrument condition met the test requirements. Initial calibration was performed before the analysis of each batch of samples, and continuous calibration verification (CCV) was inserted every 12 hours. The deviation of the middle concentration point was ≤10%, and the deviation of the lowest concentration point was ≤30%. The daughter ion with the highest signal-to-noise ratio was selected for the quantitative ion pair, and the qualitative ion pair was used for auxiliary confirmation (time consistency and ion abundance ratio matching were retained). The stability of the samples was investigated at room temperature (4 h), refrigerated storage at 4 ° C (24 h), frozen storage at −80 ° C (30 days) and freeze-thaw cycles (3 times), and the concentration change was ≤15%.

Screening of the Active Ingredients and Targets of HJD

Based on the in vitro ingredients of HJD obtained by UPLC-MS/MS, the in vitro ingredients of HJD with therapeutic effects on MAFLD were screened by literature review and combined into the blood ingredients to obtain the HJD activity fraction library. The molecular conformations of the HJD activity fraction library were obtained and their 2D data were downloaded from the PubChem database (https://pubchem.ncbi.nlm.nih.gov/). Data were imported into the SwissADME platform (http://www.swissadme.ch/) to screen for active compounds with better oral bioavailability and drug-like properties. Target prediction was performed using the Swiss Target Prediction platform (http://www.swisstargetprediction.ch/), and target proteins with Probability ≥ 0.1 were selected as potential targets of the active ingredients of HJD. And, and the target names were converted to gene names using the UniProt database (https://www.uniprot.org/). Finally, a network of HJD active ingredients and target genes was constructed using Cytoscape3.10.0 software.

Acquisition of Microarray Data and Identification of DEGs

Using “Metabolic-associated fatty liver disease” as the search term, we retrieved from the NCBI GEO public repository (https://www.ncbi.nlm.nih.gov/geo), screened by sequencing type (array analysis), animal species (Homo sapiens) and sample source (tissue), and finally obtained a GSE48452 from the GPL11532 platform containing 14 normal human liver tissue and 18 MAFLD human liver tissue. We used the R language “limma” package, and used the R language function to make a volcano map to further filter the DEGs with | log2 (fold change) |> 1 and p-value <0.05 and form a heatmap.

MAFLD-Related Target Screening

With “Nonalcoholic fatty liver disease” and “metabolic associated fatty liver disease” as keywords in GeneCards(https://www.genecards.org/), Drug Bank (https://go.drugbank.com/), OMIM(https://www.omim.org/), TTD(https://db.idrblab.net/ttd/), and NCBI(https://www.ncbi.nlm.nih.gov/) databases, collecting disease targets associated with MAFLD. The targets collected from the five databases were merged and removed as MAFLD target libraries. The UniProt database was used to standardize the disease target into a gene name, namely the MAFLD disease target.

Potential Targets for HJD Treatment of MAFLD

Combining the differential gene of 2.5 and the MAFLD disease target of 2.6 and intersection with the ingredient potential target of 2.4 is a potential target for HJD treatment of MAFLD.

Protein-Protein Interaction (PPI) Network Construction

The above intersection targets were imported into the STRING database (https://cn.string-db.org/), and the protein species was selected “Homo sapiens”, with a protein interaction score higher than 0.4. All other parameters were set to their default values. The unconnected nodes in the hidden network formed the PPI network. The data were imported into Cytoscape software (version 3.10.0) for visualization processing, and a PPI network map was constructed based on the size of the nodes and color depth. The MCODE plugin was used to classify and analyze the target interaction relationship, and the core targets in the PPI network were extracted.

The Analysis of KEGG and GO

To facilitate enrichment analysis, valid targets for HJD therapy of MAFLD were added into the Metascape database (https://metascape.org/). A threshold of P <0.01 was established to screen the relevant KEGG and GO entries. Biological processes (BP), cellular ingredients (CC), and molecular functions (MF) were all included in the GO study. The bioinformatics cloud platform (https://www.bioinformatics.com.cn) was used to create the KEGG and GO enrichment analysis maps, and the analysis findings were sorted from large to small based on log10 (P) values.

Molecular Docking

Initially, active ingredients were screened if their median value in the active ingredient-effective target interaction network was larger than or equal to twice the median. The two-dimensional structure of the active ingredient was obtained from the PubChem website, and the Chem3D program was used to convert it into the three-dimensional structure with the lowest free energy. The PDB database was then used to find the core target in the MCODE subcluster with degree values more than or equal to double median, and the "PyMOL" program was used to remove the water molecules and small molecule ligands. After that, the protein and medication ingredient were converted into PDBQT format files and active pockets were found using the "Auto DockTools" program. Ultimately, we performed molecular docking using the "vina" program. The binding energy was calculated according to the formula below.

$$\Delta G_{bind} = \Delta G_{vdW} + \Delta G_{H-bond} + \Delta G_{elec} + \Delta G_{desolv} + \Delta G_{tors} - T\Delta S$$

Cell Culture and Treatment

HepG2 cells were grown in Dulbecco's modified Eagle Medium (DMEM; Gibco, USA), which was enhanced with 10% FBS (fetal bovine serum, Gibco), 100μg/mL penicillin, and 100μg/mL streptomycin. The culture was maintained at 37 °C in a humidified environment with 95% air and 5% CO2. After incubating HepG2 cells with 0.25 mm FFAs for 24 hours to promote lipid formation, the various groups were treated to varying concentrations of HJD (40, 80, and 160 ng/mL) and silibin solution (50μM). DMEM in the same volume was administered to the FFA group and the control group.

Oil Red O Staining

10% paraformaldehyde was employed to fix the cells. Following three PBS washes, the cells were stained for 20 minutes using the oil red working solution. After being washed with staining washes, nuclei were stained with hematoxylin staining solution. The HepG2 cells were inspected under a 200 × magnification microscope.

ELISA

The cells were removed from each group and then subjected to two PBS washes. Using ELISA, the expression levels of TC, TG, FFA, NO, and ROS were determined in compliance with the manufacturer's recommendations.

WB

Using the Radio Immunoprecipitation Assay (RIPA) lysate Buffer, protein extracts were obtained from HepG2 cells and subsequently separated on 10% SDS-PAGE gels. After that, gels were placed onto polyvinylidene difluoride (PVDF) membranes, which were then incubated at 4 °C for a whole night with primary antibodies against CASP3, BCL2, RAGE, β-actin, and GAPDH. After being cleaned, the PVDF membranes were incubated for one hour at room temperature with secondary antibodies. Ultimately, chemiluminescence was used to create protein blots on the membrane.

RT-PCR

Reverse transcription: 25°C for 5 minutes, 42°C for 30 minutes, 85°C for 5 minutes, and 4°C for 5 minutes; 20 μL PCR reaction system was set up using an RT-PCR kit; reaction conditions included predenaturation at 95°C for 15 minutes, denaturation at 95°C for 10 seconds, annealing at 60°C for 30 seconds, cycling 40 times, and repeating a single sample three times. Following the amplification procedure, Ct values were assessed. Fluorescence quantitative PCR relative quantitative analysis 2-ΔΔ Ct was used for statistical analysis, with GAPDH serving as an internal reference. Table 2

Table 2 Primer Sequences

Primer Name	FORWARD	REVERSE	Length /bp
CASP3	GTGGAGGCCGACTTCTTGTATGC	TGGCACAAAGCGACTGGATGAAC	100
BCL2	TACGAGTGGGATGCGGGAGATG	CCGGGCTGGGAGGAGAAGATG	80
RAGE	ACCGAGTCCGTGTCTACCAGATTC	CCATCCAAGTGCCAGCTAAGAGTC	145

displays the primer sequences. The Guangzhou-based RiboBio Company developed and produced the primers. The expression levels of CASP 3, BCL 2, and RAGE were found.

Statistical Analysis

SPSS 22 software was used for data analysis. Measurement data were expressed as mean ± standard deviation (± s) when in accordance with normal distribution. One-way ANOVA was used for comparison among multiple groups when the data were in accordance with normal distribution, and Tukey's test was used for pairwise comparison when the data were in accordance with homogeneity of variance. When variances were not homogeneous, the Dunnett T3 test was used. When the data did not conform to the normal distribution, the nonparametric Kruskal–Wallis test was used. $P < 0.05$ was considered statistically significant.

Results

Analysis of HJD Blood Ingredients

According to "2.2", the ingredients in vitro, plasma and blank plasma samples of HJD were analyzed by full scanning in positive and negative ion modes to obtain the Total ions current (TIC), as shown in Figure 1. Based on the primary and secondary fragment ion information of the compounds and comparing relationship between the total ion current maps above, 78 chemical ingredients (Table 3) including 11 phenolic acids, 11 Flavonoids, 3 Quinones, 3 Lignans and Coumarins, 1 Tannins, 2 Alkaloids, 35 Terpenoids, 4 Organic acids, and 8 Others. In order to further understand the structure of compounds based on effective substances contained in HJD, by comparing the information of terpenoids represented by ginsenoside Rg 1, phenolic acids represented by caffeic acid, flavonoids represented by isoquercitrin and organic acids represented by succinate in HJD, combined with the references and database, the secondary mass spectrogram the and mode of cleavage is shown in Figure 2.

Acquisition of Effective Targets for HJD Against MAFLD

Table 2's blood ingredients (band *) and MAFLD therapeutic effects (band #) were integrated to create a HJD active ingredient library of 64 compounds. After the compounds were added to the Swiss Target Prediction platform, 355 targets were found by screening for target proteins with Probability > 0.1. The "Cytoscape" program then built the HJD regulatory network after translating the target names to gene names. The larger the node and the deeper the color in Figure 3a, which indicates the larger the node degree value—that is, the stronger the influence on the disease—the more so. Eleven ingredients in the network had degree values larger than or equal to twice the median of the active ingredient degree values (twice the median of degree values = 30), as shown in Table 4. This suggests that these ingredients might be the main active ingredients for the HJD therapy of MAFLD. As seen in Figure 3b, a total of 2005 DEGs were found in GSE48452, comprising 1006 upregulated and 999 downregulated genes by the R language. A few of the highlighted genes are also able to be seen on the volcanic map. The 27 genes with $P < 0.05$ and $|\log 2 \text{ fold change}| \geq 1$ are shown in Figure 3c. Figure 3d illustrates the intersection of the 1673, 5,783,38, and 336 therapy targets that were found in GeneCards, Drug Bank, OMIM, TTD, and NCBI. As seen in Figure 3e, 122 effective targets for HJD for MAFLD were obtained by integrating 27 differential genes with all therapeutic targets and then intersecting these targets with possible targets of active ingredients.

Table 3 UPLC-MS/MS Identification of HJD in vitro Ingredients and Drug-Containing Plasma

Peak Number	t R (Min)	Compounds	Formula	Molecular Weight	CAS	Ionization Model	Origin
1	1.88	Gallic acid#	C7 h6 O5	170.0215	149–91-7	[M-H]-	Polygonum cuspidatum
2	2.50	Protocatechuic acid#	C7 h6 O4	154.0266	99–50-3	[M-H]-	Hawthorn, Polygonum cuspidatum
3	2.68	Chlorogenic acid#	C16 h18 O9	354.0951	327–97-9	[M-H]-	Hawthorn
4	2.95	2,4-Dihydroxybenzoic acid*	C7 h6 O4	154.0266	89–86-1	[M-H]-	-
5	9.05	Caffeic acid#	C9 h8 O4	180.0423	331–39-5	[M-H]-	Hawthorn, Curcuma
6	10.75	Ferulic acid#	C10 h10 O4	194.0579	537–98-4	[M-H]-	Hawthorn
7	4.09	Methyl 4-hydroxybenzoate*	C8 h8 O3	152.0473	99–76-3	[M-H]-	-
8	3.30	3,5-Dihydroxyacetophenone*	C8 h8 O3	152.0473	51863–60-6	[M-H]-	-
9	3.40	5-Acetylsalicylic acid*	C9 h8 O4	180.0423	13110–96-8	[M+H]+	-
10	3.59	6-O-Galloylsalicin*	C20 h22O11	438.1162	-	[M-H]-	-
11	4.95	4-Methoxysalicylic Acid*	C8 h8 O4	168.0423	2237–36-7	[M-H]-	-
12	3.10	Catechin#	C15 h14 O6	290.079	154–23-4	[M+H]+	Hawthorn, Polygonum cuspidatum
13	3.37	Epicatechin#	C15 h14 O6	290.079	490–46-0	[M+H]+	Hawthorn
14	4.01	Isoquercitrin#	C21 h20 O12	464.0955	482–35-9	[M+H]+	Hawthorn, Polygonum cuspidatum
15	4.01	Hyperin*	C21 h20 O12	464.0955	482–36-0	[M+H]+	Hawthorn, Polygonum cuspidatum
16	3.99	Isohyperoside*	C21 h20 O12	464.0955	35589–21-0	[M+H]+	Hawthorn, Polygonum cuspidatum
17	4.66	Aromadendrin*	C15 h12 O6	288.0634	480–20-6	[M+H]+	-
18	3.48	Orientin	C21 h20 O11	448.1006	28608–75-5	[M+H]+	Hawthorn
19	3.61	Rutin#	C27 h30 O16	610.1534	153–18-4	[M+H]+	Polygonum cuspidatum
20	3.83	Vitexin#	C21 h20 O10	432.1056	3681–93-4	[M+H]+	Hawthorn
21	3.47	Isoorientin#	C21 h20 O11	448.1006	4261–42-1	[M+H]+	Hawthorn
22	3.83	Isovitexin#	C21 h20 O10	432.1056	38953–85-4	[M+H]+	Hawthorn
23	9.63	Emodin#	C15 h10 O5	270.0528	518–82-1	[M-H]-	Polygonum cuspidatum
24	5.62	Aloe emodin#	C15 h10 O5	270.0528	481–72-1	[M+H]+	Polygonum cuspidatum
25	9.63	Emodin-8-methyl ether*	C16 h12 O5	284.0685	3774–64-9	[M-H]-	Polygonum cuspidatum
26	5.75	7-Methoxycoumarin*	C10 h8 O3	176.0473	531–59-9	[M+H]+	-
27	5.26	Decursinol*	C14 h14 O4	246.0892	23458–02-8	[M+H]+	-
28	5.75	8-(3-hydroxyisopentyl)-7-methoxycoumarin	C15 h18 O4	262.1205	69219–24-5	[M+H]+	-
29	2.76	Procyanidin B1#	C30 h26 O12	578.1424	20315–25-7	[M-H]-	Hawthorn
30	0.89	Trigonelline#	C7 h7 NO2	137.0477	535–83-1	[M+H]+	-
31	2.35	p-Coumaroylputrescine*	C13 h18 N2 O2	234.1368	34136–53-3	[M+H]+	-
32	7.75	Curcumenol#	C15 h22 O2	234.162	19431–84-6	[M+H]+	Curcuma
33	4.49	Ginsenoside Rg1#	C42 h72 O14	800.4922	22427–39-0	[M-H]-	Notoginseng
34	5.72	Ginsenoside Rg2#	C42 h72 O13	784.4973	52286–74-5	[M-H]-	Notoginseng
35	6.34	Ganoderic Acid A#	C30 h44 O7	516.3087	81907–62-2	[M-H]-	Ganoderma lucidum
36	6.85	Ganoderenic acid D*	C30 h40 O7	512.2774	-	[M+H]+	Ganoderma lucidum
37	6.03	Ganoderic Acid J	C30 h42 O7	514.2931	-	[M+H]+	
38	4.33	Notoginsenoside R1#	C47 h80 O18	932.5345	80418–24-2	[M-H]-	Notoginseng
39	5.85	Ginsenoside Rh1#	C36 h62 O9	638.4394	63223–86-9	[M-H]-	Notoginseng
40	5.42	Notoginsenoside Rb1*	C54 h92 O23	1108.6029	-	[M-H]-	Notoginseng
41	4.49	Ginsenoside Rh4*	C36 h60 O8	620.4288	174721–08-5	[M+H]+	Notoginseng
42	4.46	Ginsenoside Re*	C48 h82 O18	946.5501	52286–59-6	[M-H]-	Notoginseng
43	6.96	Ganoderic Acid F	C32 h42 O9	570.2829	-	[M+H]+	Ganoderma lucidum
44	6.29	Ganoderenic Acid G	C30 h40 O7	512.2774	-	[M+H]+	Ganoderma lucidum
45	6.27	Ganoderenic acid K	C32 h44 O9	572.2985	-	[M+H]+	Ganoderma lucidum
46	7.11	Ganoderenic Acid A	C30 h42 O7	514.2931	-	[M+H]+	Ganoderma lucidum
47	6.20	Lucidenic Acid N	C27 h40 O6	460.2825	-	[M+H]+	Ganoderma lucidum
48	7.77	Ganoderic Acid DM	C30 h44 O4	468.324	173075–45-1	[M+H]+	Ganoderma lucidum
49	7.54	Atractylenolide III*	C15 h20 O3	248.1412	73030–71-4	[M+H]+	-
50	6.04	Telekin*	C15 h20 O3	248.1407	6752–90-5	[M+H]+	-
51	3.26	Ridentin*	C15 h20 O4	264.1362	28148–84-7	[M+H]+	-
52	8.27	Alisol H	C30 h46 O4	470.3396	-	[M+H]+	Rhizoma Alismatis

(*Continued*)

https://doi.org/10.2147/DMSO.S506350

Table 3 (Continued).

Peak Number	t R (Min)	Compounds	Formula	Molecular Weight	CAS	Ionization Model	Origin
53	5.87	Lucidenic Acid G*	C27 h40 O7	476.2774	-	[M+H]+	Ganoderma lucidum
54	5.80	Ginsenoside Rb1#	C54 h92 O23	1108.6029	41753–43-9	[M-H]-	Notoginseng
55	5.04	Ganoderic Acid N*	C30 h42 O8	530.288	-	[M+H]+	Ganoderma lucidum
56	7.25	Alisol C	C30 h46 O5	486.3345	30489–27-1	[M+CH3COOH-H]-	Rhizoma Alismatis
57	8.91	Curcumol#	C15 h24 O2	236.1776	4871–97-0	[M+H]+	Curcuma
58	9.05	Alisol E 23-Acetate*	C32 h52 O6	532.3764	155301–58-9	[M+CH3COOH-H]-	Rhizoma Alismatis
59	9.73	Germacrone#	C15 h22 O	218.1671	6902–91-6	[M+H]+	Curcuma
60	9.25	Maslinic acid#	C30 h48 O4	472.3553	4373–41-5	[M-H]-	Hawthorn
61	9.25	Corosolic acid#	C30 h48 O4	472.3553	4547–24-4	[M-H]-	Hawthorn
62	8.32	Alisol C 23-acetate	C32 h48 O6	528.3451	26575–93-9	[M+CH3COOH-H]-	Rhizoma Alismatis
63	8.90	Alisol A	C30 h50 O5	490.3658	19885–10-0	[M+H]+	Rhizoma Alismatis
64	9.51	Alisol A 24-acetate#	C32 h52 O6	532.3764	18674–16-3	[M-H]-	Rhizoma Alismatis
65	8.42	Alisol F#	C30 h48 O5	488.3502	155521–45-2	[M+CH3COOH-H]-	Rhizoma Alismatis
66	10.81	Ursolic acid#	C30 h48 O3	456.3603	77–52-1	[M-H]-	Hawthorn
67	0.98	Citric Acid	C6 h8 O7	192.027	77–92-9	[M-H]-	-
68	1.44	Succinic acid#	C4 h6 O4	118.0266	110–15-6	[M-H]-	Rhizoma Alismatis
69	1.22	Malonic acid*	C3 h4 O4	104.011	141–82-2	[M-H]-	-
70	2.08	Trans-2-Butene-1,4-dicarboxylic Acid*	C6 h8 O4	144.0423	4436–74-2	[M+H]+	-
71	0.9	Epigoitrin#	C5 h7 NOS	129.0248	1072–93-1	[M+H]+	-
72	4.54	2-Methyl-5-acetonyl-7-hydroxychromone*	C13 h12 O4	232.073	28955–30-8	[M+H]+	-
73	2.95	Isobiflorin*	C16 h18 O9	354.0951	152041–16-2	[M+H]+	-
74	2.95	Resveratroloside*	C20 h22 O8	390.1315	38963–95-0	[M-H]-	Polygonum cuspidatum
75	3.86	Piceid#	C20 h22 O8	390.1315	27208–80-6	[M-H]-	Polygonum cuspidatum
76	2.70	Leucopelargonidin*	C15 h14 O6	290.079	520–17-2	[M+H]+	-
77	5.24	4-Methoxybenzaldehyde*	C8 h8 O2	136.0524	123–11-5	[M+H]+	-
78	4.54	Resveratrol#	C14 h12 O3	228.0786	501–36-0	[M+H]+	Polygonum cuspidatum

Notes: Band # is the ingredient with therapeutic effect of MAFLD, and * is the ingredient of HJD blood entry. In particular, all ingredients detected by HJD in blood can be detected in vitro.

PPI Network Construction and Functional Enrichment Analysis of Effective Targets

As seen in Figure 4a, the intersection targets were imported into the STRING website for PPI analysis, yielding PPI networks with 122 nodes and 2052 edges. The tighter the protein contact, the bigger the node and the deeper the color, the more edges there are. Table 5 displays the ordering of targets and degree values. It suggests that these targets might be the main targets of HJD for treating MAFLD. Figure 4b illustrates the core target concept network. Of the 16 targets, two are larger than or equal to the median of degree values. Figure 5c and d display the KEGG pathway enrichment and GO function analysis of the legitimate targets according to the Metascape database. The top 10 signaling pathways for HJD therapy in MAFLD are displayed in Figure 4c. These pathways include the AGE-RAGE signaling pathway, EGFR tyrosine kinase inhibitor resistance, lipid and atherosclerosis, etc. Figure 4d data indicate that the primary biological mechanisms at play are positive control of cell migration, response to xenobiotic stimulation, and hormone response. Membrane raft, vesicle lumen, side of membrane, etc. were the principal cell components involved. The primary molecular processes entailed are nuclear receptor activity, oxidoreductase activity, and protein kinase activity. Figure 4e depicts the link between the key pathway and the effective target. From this relationship, a pathway that is most pertinent to the disease and effective target is chosen, and Figure 4f displays its pathway diagram.

Molecular Docking

The 11 active ingredients with a median value greater than or equal to twice the median value of the HJD active ingreditor-effective target interaction network were docked with 16 core targets with a median value greater than or equal to twice the median value of the PPI network, and 176 sets of docking results were obtained, as shown in Figure 5a. Among them, there were 161 groups (91.5%) of active ingredients with binding energies less than −5.0 kcal·mol-1. There were 99 sets of binding

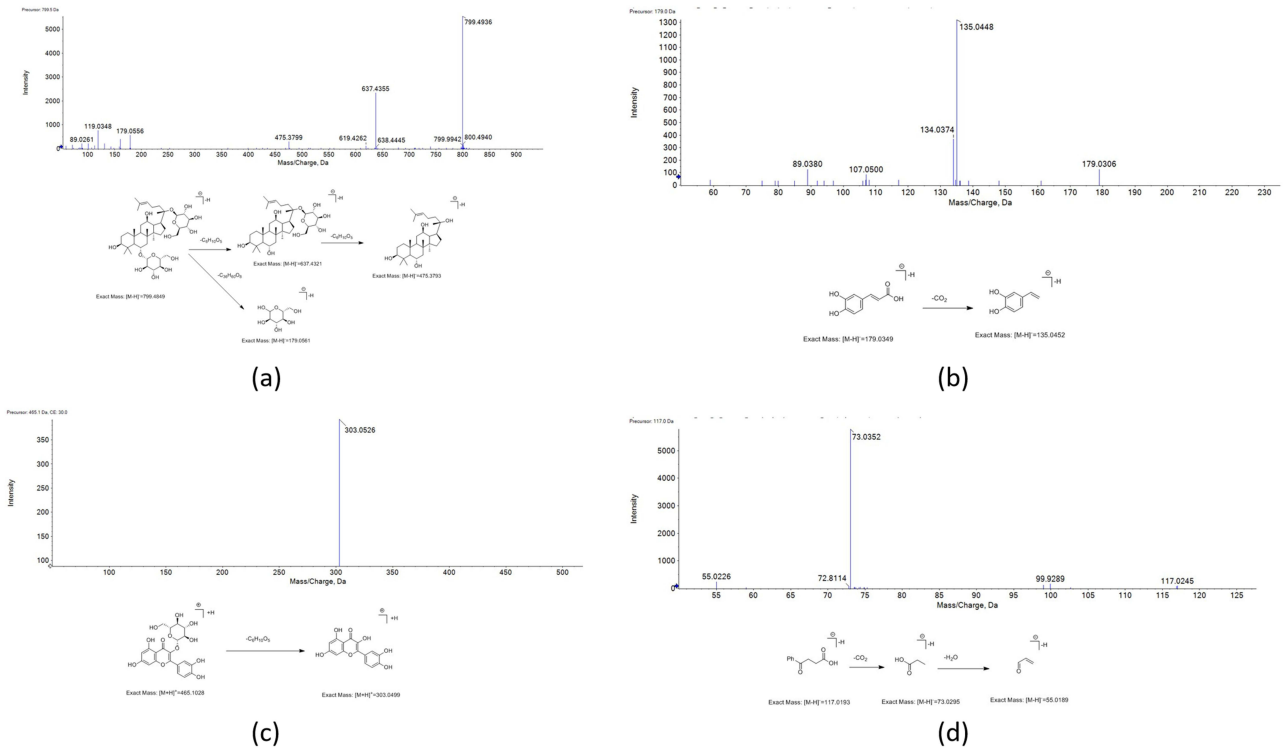

Figure 2 The secondary mass spectrogram and mode of cleavage in HJD. (**a**) Ginsenoside Rg1. (**b**) Caffeic acid. (**c**) Isoquercitrin. (**d**) Succinic acid.

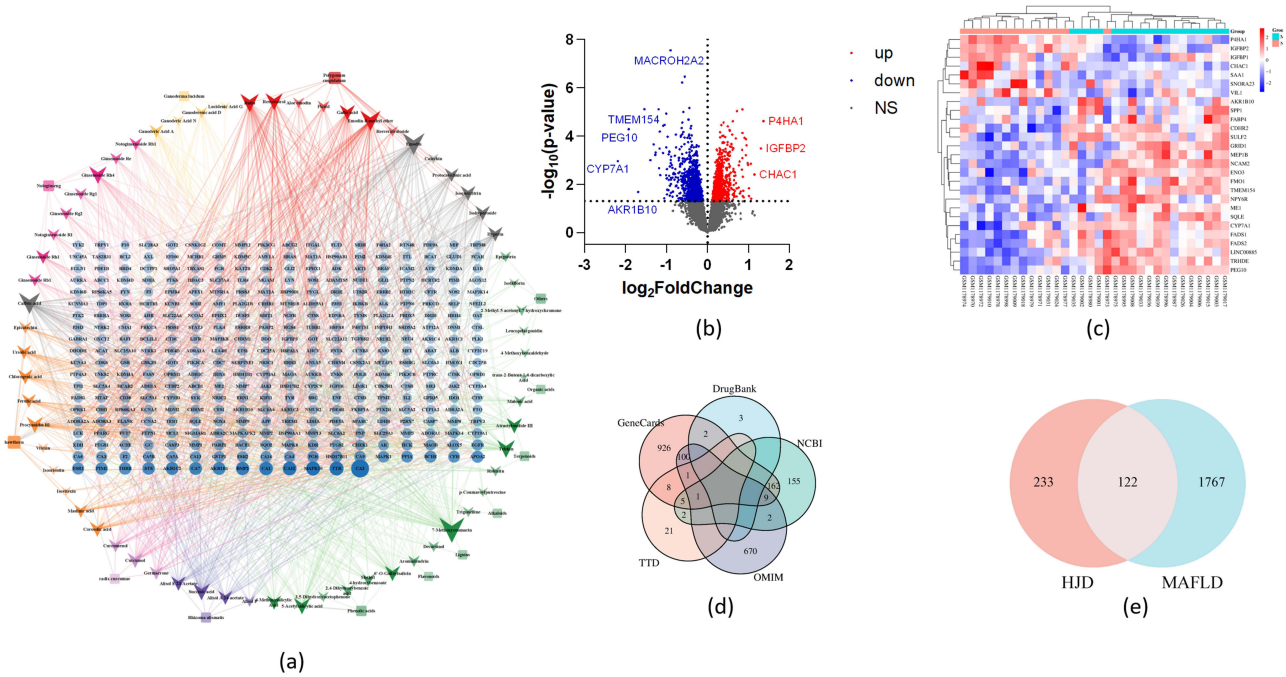

Figure 3 Acquisition of effective targets for HJD treatment of MAFLD. (**a**) Active ingredient-target network diagram of HJD, the "V" shape is the active ingredient of HJD, different colors represent different drugs, the gray is the ingredients belonging to 2 or more traditional Chinese medicines, and the green is the unattributed ingredients. The middle blue circle is the target genes. (**b**) Volcano plot of the DEGs. (**c**) Heatmap of the DEGs. (**d**) The therapeutic targets for MAFLD. (**e**) Effective HJD targets for MAFLD treatment.

https://doi.org/10.2147/DMSO.S506350

Table 4 Major Active Ingredients of HJD Treatment for MAFLD

Degree	Compounds	CAS	Origin	Class	Peak Area
67	7-Methoxycoumarin	531–59-9	-	Lignans and Coumarins	1332459.92
53	Emodin	518–82-1	Polygonum cuspidatum, Rhizoma alismatis	Quinones	599162.74
51	Caffeic acid	331–39-5	Hawthorn, radix curcumae	Phenolic acids	2785295.23
46	Emodin-8-methyl ether	3774–64-9	Polygonum cuspidatum	Quinones	29662.01
39	Rutin	153–18-4	Polygonum cuspidatum	Flavonoids	138086.56
36	Telekin	6752–90-5	-	Terpenoids	703322.06
35	Ginsenoside Rh4	174721–08-5	Notoginseng	Terpenoids	7888311.18
34	Resveratrol	501–36-0	Polygonum cuspidatum	Others	163889.30
33	Succinic acid	110–15-6	Rhizoma alismatis	Organic acids	60993884.03
30	Procyanidin B1	20315–25-7	Hawthorn	Tannins	196365.32
30	5-Acetylsalicylic acid	13110–96-8	-	Phenolic acids	791994.00

energies less than −7.0 kcal·mol-1, accounting for 56.3%. These results indicated that the potential active ingredients screened had good binding affinity between the core targets. Partial receptor-ligand binding patterns are shown in Figure 6b–e.

Effect of HJD on Lipid Accumulation and Biochemical Indexes of HepG2 Cells in the MAFLD Model

As seen in Figure 6a. After being exposed to 0.25 mm FFA for 24 hours, HepG2 cells exhibiting big fat particles stained redder than the control group. When compared to the FFA group without HJD, the silibin group and the low, medium, and high dosage HJD groups displayed considerably reduced lipid content, suggesting that HJD has an inhibitory impact on lipid accumulation. As seen in Figure 6b. FFA, TC, and TG were considerably higher in the model group (P <0.01) as compared to the control group, suggesting that the in vitro model of MAFLD was successfully established. In the silibin group and HJD group, FFA, TC, and TG were dramatically lowered (P <0.01) compared to the model group, while NO rose significantly (P <0.01), suggesting that HJD has the effect of alleviating MAFLD in vitro model.

Validation of the Related Pathways

As demonstrated in Figure 7a, the FFA group's protein expression of RAGE and CASP3 was substantially higher ($P < 0.01$) than that of the control group, whereas BCL2's protein expression was significantly lower ($P < 0.01$) than that of the former. In the silibin group and the low, middle, and high dosage HJD group, there was a substantial down-regulation ($P < 0.01$) of CASP3 and RAGE protein expression compared to the FFA group, and a significant up-regulation ($P < 0.01$) of BCL2 protein expression. According to Figure 7b, the mRNA expression in the RTPCR experiment confirmed the WB data. Figure 7c illustrates that the FFA group had a significant decrease in NO ($P < 0.01$) and an increase in ROS ($P < 0.01$) compared to the control group; additionally, the silibin group and HJD low, middle, and high dose groups had a significant increase in NO ($P < 0.01$) and a significant reduction in ROS ($P < 0.01$) compared to the FFA group. As seen in Figure 7d, the FFA group's apoptosis rate was substantially higher ($P < 0.01$) than that of the control group. The apoptosis rate of the silibin group and the HJD low, medium, and high dosage groups was considerably lower ($P < 0.01$) than that of the FFA group. In conclusion, combined with Figure 4f, HJD may down-regulating RAGE protein on the membrane to reduce the production of ROS, promote the synthesis of NO by NOS, mediate proteins related to BCL2/CASP3 apoptosis pathway, inhibit the apoptosis of normal cells, and then improve the symptoms of MAFLD.

Discussion

As social economies have grown, MAFLD has emerged as one of the major global public health issues. This condition is quite common in China, where it is the leading source of abnormal liver biochemical indicators in health examinations as well as the leading cause of chronic liver disease. Despite the fact that MAFLD has been the subject of much fundamental study both domestically and internationally, the precise etiology of the illness and the major targets of fat energy metabolism control remain unclear, and there is currently no approved medication that may fully treat MAFLD.

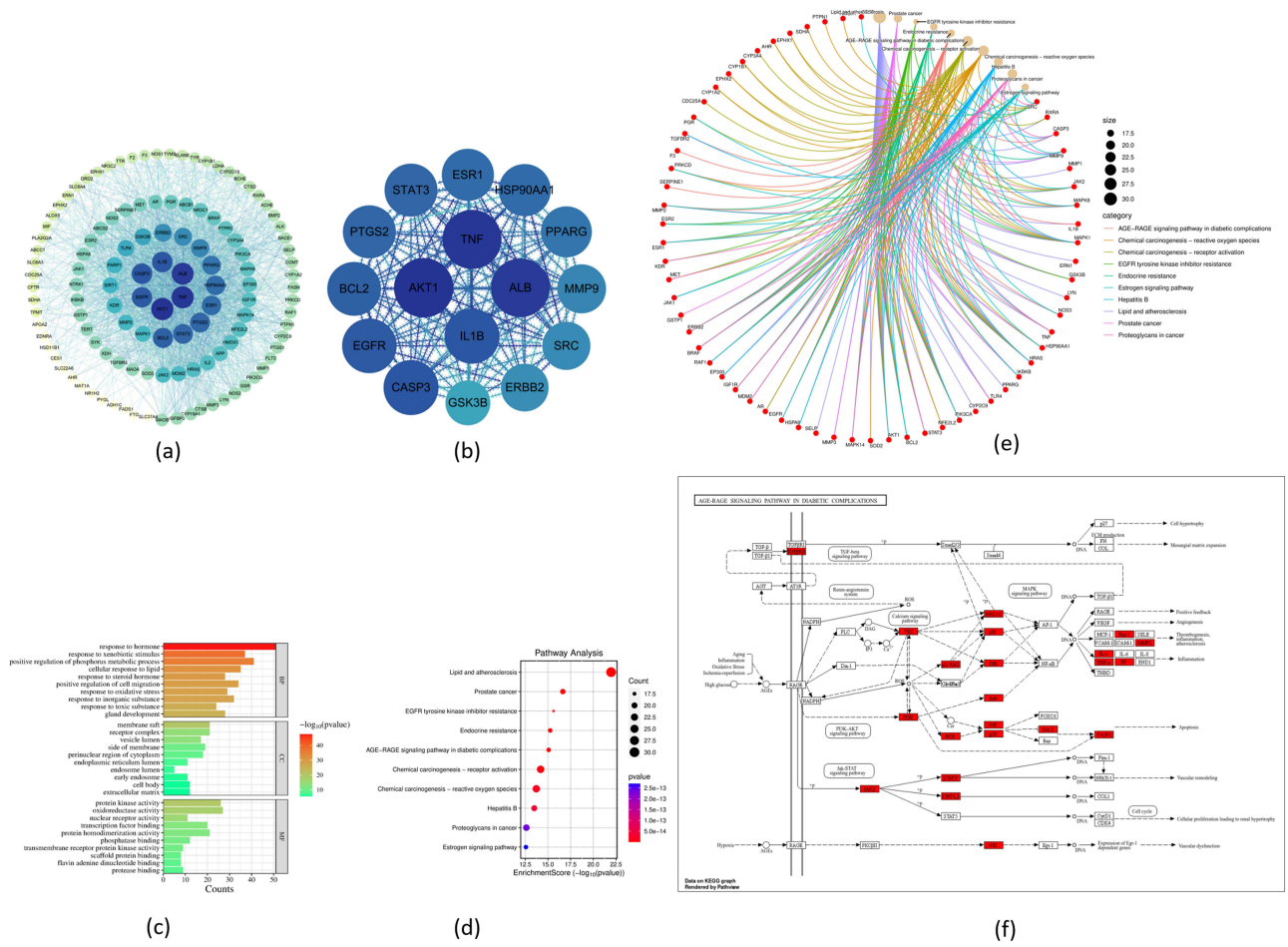

Figure 4 PPI network construction and functional enrichment analysis of the effective targets. (**a**) Analysis results of the PPI network. (**b**) Core targets of the PPI network. (**c**) GO analysis of the effective targets. (**d**) KEGG analysis of the effective target. (**e**) The relationship between the effective targets and the key pathways. (**f**) AGE-RAGE pathway map, with the marker red gene as the effective gene for HJD treatment of MAFLD (the labeled red module is the effective target of HJD in the treatment of MAFLD).

Some researchers[19] propose that MAFLD may be the result of parallel strikes by multiple factors, namely "multiple (parallel) hits" theory. This theory suggests that many factors, including insulin resistance, adipose tissue dysfunction, mitochondrial dysfunction, endoplasmic reticulum stress, fatty acid, intestinal flora, dietary factors, and genetic and

Table 5 Key Target Prediction of HJD Treatment for MAFLD

Number	Target	Degree Values	UniProt ID
1	AKT1	93	P31749
2	TNF	92	P01375
3	ALB	91	P02768
4	CASP3	82	P42574
5	IL1B	82	P01584
6	EGFR	81	P00533
7	BCL2	79	P10415
8	STAT3	77	P40763
9	PTGS2	77	P35354
10	HSP90AA1	75	P07900

(*Continued*)

https://doi.org/10.2147/DMSO.S506350

Table 5 (Continued).

Number	Target	Degree Values	UniProt ID
11	ESR1	75	P03372
12	PPARG	72	P37231
13	MMP9	67	P14780
14	SRC	65	P12931
15	ERBB2	64	P04626
16	GSK3B	57	P49841

epigenetic factors, work together to induce the occurrence and progression of MAFLD,[20] and the theory of "multiple (parallel) hits" is gradually being widely accepted.[6] The theory of "multiple (parallel) hits" coincides with the overall treatment of TCM, perhaps traditional Chinese medicine is a new way to treat MAFLD. Under this research background, because the variety of chemical ingredients of TCM prescriptions can play a wide range of pharmacological activities, the advantages of multi-target regulation and overall treatment of TCM are fully demonstrated. However, in the development process of TCM modernization, TCM prescriptions are faced with the problems of complex prescription and large prescription volume, and it is difficult to clarify the key substance basis,[21] Then for the efficient development of modern preparations and quality control brought great resistance. In light of this issue, system pharmacology has advanced significantly in the last several years. Its primary objective is to use a combination of systems biology, computer simulation, multi-omics, and other technologies to uncover the interaction relationship between several active ingredients and multiple proteins during the treatment process from the standpoint of the system level and overall biological network. Realizing the shift from empirical to evidence-based medicine is anticipated.[22] In this paper, we analyzed the mechanism and substance basis of HJD treatment in MAFLD by UPLC-MS/MS technology, network pharmacology, bioinformatics analysis, molecular docking and other means, and verified the mechanism of HJD treatment in MAFLD by WB, PCR and flow cytometry.

HJD is an oral decoction, which has various medicinal flavors and complicated decoction process. If we directly use the online database of Chinese medicine ingredients to screen Chinese medicine ingredients, it may not consider the dose-effect relationship, the changes of ingredients in the process of Chinese medicine decoction, the medicinal parts of Chinese medicine and other factors,[23] In flu affect the results of a series of network pharmacological analysis. Therefore,

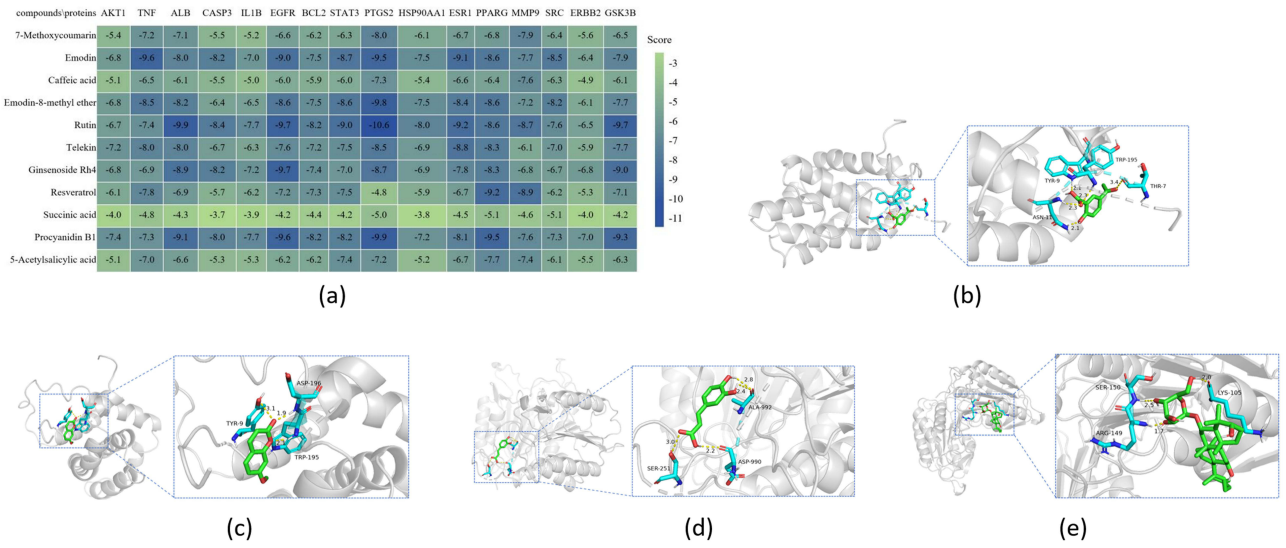

Figure 5 Molecular Docking. (**a**) Heatmap of the binding energy obtained from the molecular docking results. (**b**) 5-Acetylsalicylic acid-BCL2. (**c**) 7-Methoxycoumarin-BCL2. (**d**) Caffeic acid-CASP3. (**e**) Ginsenoside Rh4-CASP3.

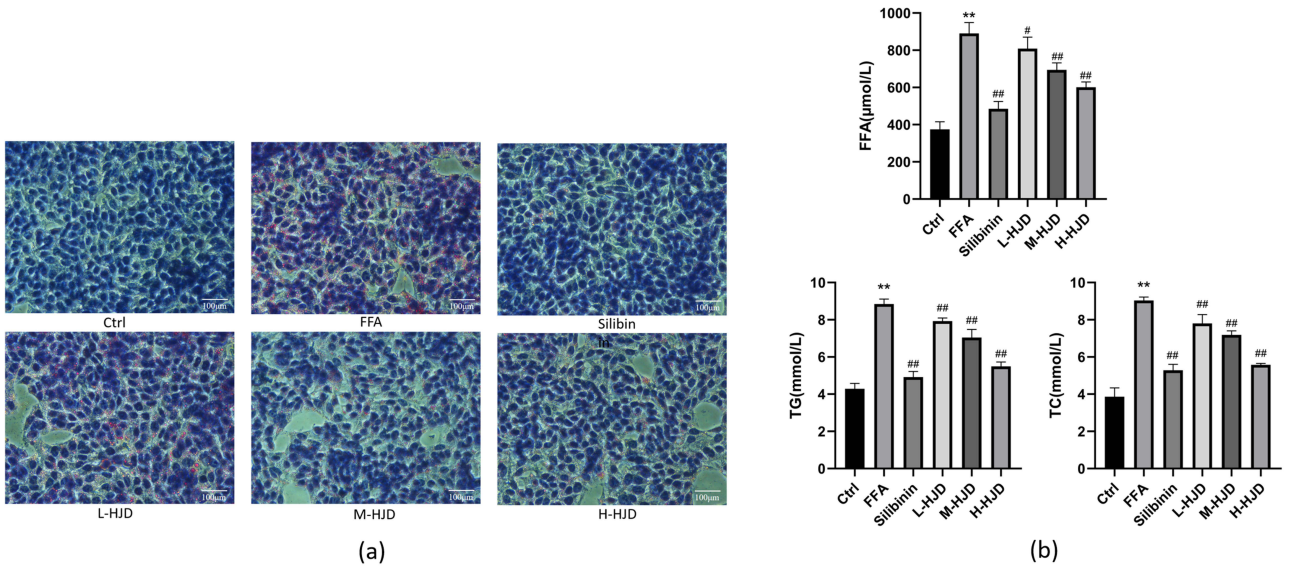

Figure 6 Effect of HJD on lipid accumulation and biochemical indexes in HepG2 cells in MAFLD model. (**a**) Oil red O staining in HepG2 cells. Magnification ratio: 200. (**b**) Effect of HJD on the biochemical index of HepG2 cells (n=6). FFA, human free fatty acid; TG, human triglyceride; TC, human total cholesterol; Ctrl was the control group; FFA was the model group; silibin was the silibin group; L-HJD was the HJD low-dose group; M-HJD was the HJD middle-dose group; H-HJD was the HJD high-dose group. Compared with Ctrl, * * *P*<0.01; Compared with FFA, # *P* <0.05, # # *P* <0.01.

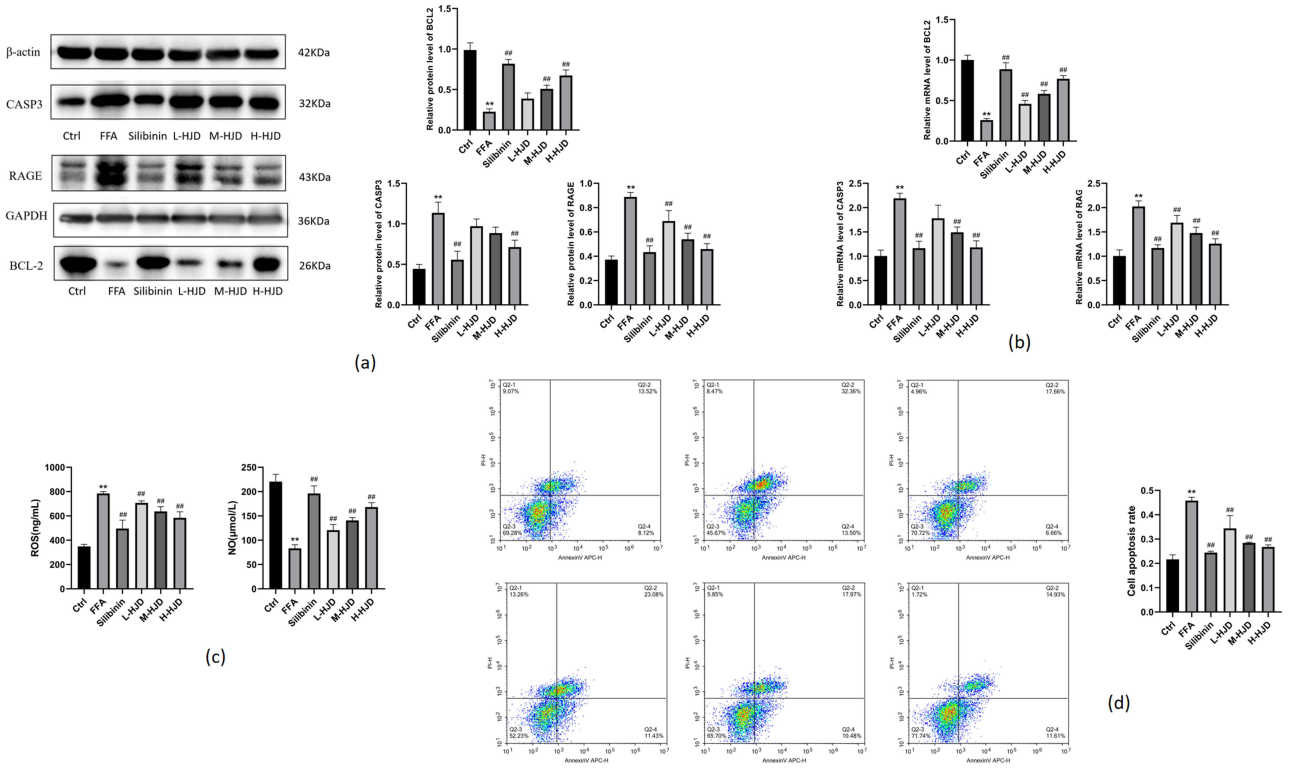

Figure 7 Validation of the related pathways. (**a**) Effect of HJD on protein expression in the MAFLD model of HepG2 cells (n=3). (**b**) Effect of HJD on mRNA expression in the MAFLD model of HepG2 cells (n=6). (**c**) Effect of HJD on NO and ROS in the MAFLD model of HepG2 cells (n=6). (**d**) Effect of HJD on apoptosis in the MAFLD model of HepG2 cells. NO, human nitric oxide; ROS, human reactive oxygen species (n=6). Ctrl was the control group; FFA was the model group; silibin was the silibin group; L-HJD was the HJD low-dose group; M-HJD was the HJD middle-dose group; H-HJD was the HJD high-dose group. Compared with Ctrl, * * *P*<0.01; Compared with FFA, # # *P* <0.01.

https://doi.org/10.2147/DMSO.S506350

the UPLC-MS/MS technology was used to construct the active ingredient library of HJD. Another problem affecting the accuracy of network pharmacology research is the content of ingredients. When the content of the predicted effective ingredients in the prescription is too low, they cannot be identified as disease-resistant ingredients. It is necessary to judge the potential ingredients by combining the content analysis. Among the 11 core ingredients screened in this study, the top five contents were Succinic acid, Ginsenoside Rh4, Caffeic acid, 7-Methoxycoumarin, and 5-Acetylsalicylic acid. Among the five core ingredients, Succinic acid, Ginsenoside Rh4, and Caffeic acid showed significant anti-MAFLD effects. Remaxol containing Succinic acid shows antioxidant and cytoprotective activities and can be regarded as a promising metabolic hepatoprotective agent for the treatment of non-alcoholic fatty liver disease;[24,25] Yang[26] found that Ginsenoside Rh4 Improves Hepatic Lipid Metabolism and Inflammation in a Model of MAFLD by Targeting the Gut Liver Axis and Modulating the FXR Signaling Pathway; Hong[27] and Zhang[28] used Caffeic acid to improve MAFLD by regulating autophagy and activating the Keap1/Nrf2 pathway, respectively. Sandesh[29] took advantage of the strong antioxidant effect of 7-Methoxycoumarin to show good hepatoprotective activity in rats induced by CCl4. Based on the hepatoprotective effect of 7-Methoxycoumarin, it may be used in the prevention or rehabilitation of MAFLD in the future; 5-Acetylsalicylic acid as a positive control in the treatment of ulcerative colitis showed better anti-inflammatory and intestinal protection effect,[30] 5-Acetylsalicylic acid may play an important role in the treatment of MAFLD by targeting the gut-liver axis and anti-inflammation in future studies. However, among the non-core ingredients with degree values less than twice the median, some compounds, such as Trigonelline, Gallic acid, Curcumenol, Epigoitrin, Ginsenoside Rg1, also had a high relative content in the samples and had significant therapeutic effects.[31–35] Considering the above factors, Succinic acid, Ginsenoside Rh4, Caffeic acid, 7-Methoxycoumarin, 5-Acetylsalicylic acid, Trigonelline, Gallic acid, Curcumenol, Epigoitrin, Ginsenoside Rg1 and other ingredients may be the substance basis for the treatment of MAFLD.

Studies have shown that the main causes of MAFLD are insulin resistance and obesity, while MAFLD is also one of the complications of diabetes.[36] In the KEGG enrichment analysis, the AGE-RAGE signaling pathway showed a high enrichment and significance ($P < 0.05$). Meanwhile, some studies have shown that the AGE-RAGE signaling pathway has become an important therapeutic pathway in MAFLD.[37] In addition, the PPI analysis results (Table 3) showed that AKT1, TNF, ALB, IL1B, EGFR, BCL2, STAT3, and PTGS2 were the key core targets of HJD for the treatment of MAFLD (degree value =77~93). The degree values reflect the strength of the target protein interactions in the PPI network, indicating that the complex ingredients of HJD may comprehensively play the role of therapeutic MAFLD through the above targets. Combined with the analysis results of Figure 4f AGE-RAGE pathway map and PPI, it is speculated that HJD may function through the apoptotic pathway in the AGE-RAGE pathway. Studies have shown that high-fat diet and hyperglycemia increase the formation and accumulation of AGEs, and the increased AGEs drive signaling in cells downstream of RAGE, which subsequently leads to oxidative stress and chronic inflammation.[38] Besides, Li[39] found that with the time of mold making, the liver apoptosis rate in MAFLD model rats will become higher and higher, BCL2 / Bax will become smaller and CASP 8 will increase, indicating that MAFLD may be pathogenic by causing apoptosis. Combined with the result of this paper, high-fat diet leads to the production of FFA, while promoting the formation and accumulation of AGEs, and then affecting the expression of RAGE and inducing oxidative stress, thus producing a large number of ROS. ROS production can activate the apoptotic pathway, further affecting the expression of proteins such as NOS, BCL2 and CASP3, thus causing hepatocyte apoptosis and causing MAFLD. Therefore, HJD may reduce the production of ROS by reducing the expression of RAGE, regulate NOS and then increase the expression of BCL2 to inhibit the expression of CASP3, thereby reducing apoptosis and alleviating MAFLD.

Current treatments for MAFLD include lifestyle intervention, drug therapy, and surgery. Lifestyle intervention is mainly through diet control and exercise, but patients have poor compliance, and can only achieve 5–10% body weight loss, and the improvement of liver fibrosis is limited.[40] Vitamin E and pioglitazone can reduce liver fat deposition, but the improvement effect on metabolic syndrome is weak, and the safety of long-term use is controversial.[41,42] Moreover, GLP-1 receptor agonists (such as telpotide) are expensive, and their applicability in Asian population needs to be further verified. Surgery can significantly improve liver fibrosis, but it is highly invasive and only suitable for patients with severe obesity.[43] Previous studies in this project have demonstrated that HJD inhibits lipid synthesis (CPT1A↑, FAS↓, ACC↑) through activation of the SIRT1/AMPK pathway, which has metabolic regulation and anti-inflammatory effects,

and is complementary to single-target drugs such as GLP-1 agonists. In terms of efficacy, liver steatosis was reduced by 50–70% and ALT/AST levels were reduced by 40–60% in the high-dose HJD group in the animal model. In addition, hepatic and renal toxicity has not been noted in preclinical studies, whereas pioglitazone is associated with a risk of edema, and gastrointestinal side effects are common with GLP-1 agonists. Therefore, HJD has certain advantages over other drugs on the market in terms of efficacy, safety, and price in the treatment of MAFLD.

In the future, in vivo experiments will be conducted to verify the role of HJD on MAFLD, and combined with single-cell sequencing and spatial transcriptome technology, we will comprehensively analyze the regulatory network of HJD on MAFLD. Available data are limited to mouse and cell models, and human PK/PD data are lacking. Moreover, the long-term safety of HJD has not been elucidated, and rare adverse effects (such as the risk of immune activation) need to be monitored.

Conclusion

The paper explored the substance basis and mechanism of HJD in the treatment of MAFLD by systematic pharmacology techniques. The results showed that HJD may regulate the AGE-RAGE signaling pathway to treat MAFLD by acting on key targets such as RAGE, BCL2 and CASP3 through the main ingredient of Succinic acid, Ginsenoside Rh4 and Caffeic acid. This study provides a theoretical basis for further clinical application and quality control of HJD.

Abbreviations

MAFLD, Metabolic-Associated Fatty Liver Disease; HJD, Hujin Decoction; UPLC-MS/MS, Ultra performance liquid chromatography/tandem mass spectrometry; ELISA, Enzyme-linked immunosorbent assay; RAGE, Advanced glycosylation end product-specific receptor; BCL2, Apoptosis regulator Bcl-2; CASP3, Caspase-3; WB, Western Blotting; FFA, Nonesterified fatty acid; Free Fat Acid; TC, Serum total cholesterol; TG, Triglyceride; NO, Nitric oxide; ROS, Reactive Oxygen Species; DEGs, Differentially Expressed Genes; GO, Gene ontology; KEGG, Kyoto Encyclopedia of Genes and Genomes; MCODE, Molecular complex detection; PDB, Protein Data Bank; PVDF, Polyvinylidene fluoride; DMEM, Dulbecco's modified Eagle's medium; RTPCR, Reverse transcription polymerase chain reaction; PPI, Protein-protein interaction.

Data Sharing Statement

The open-access datasets are available through the following URL: https://www.ncbi.nlm.nih.gov database annotated by GPL11532 as a Series Matrix File.

Institutional Review Board Statement

The experimental protocols and procedures were approved on August 22, 2023, by the Ethics Committee for Animal Experiments of Guangzhou University of Chinese Medicine, in accordance with the Guidelines for the Care and Use of Laboratory Animals (approval code: ZYD-2023-191).

All utilized public data sets were generated by others who had obtained ethical approval. The information contained in GSE48452 is from the article PMID: 23931760. The article was approved by the institutional review board ("Ethikkommission der Medizinischen Fakulta t der Universita¨ t Kiel", D425/07, A111/99). This study conforms to the first item of Article 32 of the Measures for Ethical Review of Life Science and Medical Research Involving Human Subjects dated February 18, 2023.

Disclosure

The authors declare no conflicts of interest in this work.

References

1. Badmus OO, Hillhouse SA, Anderson CD, et al. Molecular mechanisms of metabolic associated fatty liver disease (MAFLD): functional analysis of lipid metabolism pathways. *Clin Sci*. 2022;136(18):1347–1366. doi:10.1042/CS20220572

2. Younossi ZM, Koenig AB, Abdelatif D, et al. Global epidemiology of nonalcoholic fatty liver disease-Meta-analytic assessment of prevalence, incidence, and outcomes. *Hepatology*. 2016;64(1):73–84. doi:10.1002/hep.28431
3. Younossi Z, Anstee QM, Marietti M, et al. Global burden of NAFLD and NASH: trends, predictions, risk factors and prevention. *Nat Rev Gastroenterol Hepatol*. 2018;15(1):11–20. doi:10.1038/nrgastro.2017.109
4. Powell EE, Wong VW, Rinella M. Non-alcoholic fatty liver disease. *Lancet*. 2021;397(10290):2212–2224. doi:10.1016/S0140-6736(20)32511-3
5. Byrne CD, Targher G. NAFLD: a multisystem disease. *J Hepatol*. 2015;62(1 Suppl):S47–S64. doi:10.1016/j.jhep.2014.12.012
6. Fang YL, Chen H, Wang CL, et al. Pathogenesis of non-alcoholic fatty liver disease in children and adolescence: from "two hit theory" to "multiple hit model". *World J Gastroenterol*. 2018;24(27):2974–2983. doi:10.3748/wjg.v24.i27.2974
7. Buzzetti E, Pinzani M, Tsochatzis EA. The multiple-hit pathogenesis of non-alcoholic fatty liver disease (NAFLD). *Metabolism*. 2016;65 (8):1038–1048. doi:10.1016/j.metabol.2015.12.012
8. Guo X, Yin X, Liu Z, et al. Non-alcoholic fatty liver disease (NAFLD) pathogenesis and natural products for prevention and treatment. *Int J Mol Sci*. 2022;23(24):15489. doi:10.3390/ijms232415489
9. Rong L, Zou J, Ran W, et al. Advancements in the treatment of non-alcoholic fatty liver disease (NAFLD). *Front Endocrinol*. 2022;13:1087260. doi:10.3389/fendo.2022.1087260
10. Fang J, Yu CH, Li XJ, et al. Gut dysbiosis in nonalcoholic fatty liver disease: pathogenesis, diagnosis, and therapeutic implications. *Front Cell Infect Microbiol*. 2022;12:997018. doi:10.3389/fcimb.2022.997018
11. Mun J, Kim S, Yoon HG, et al. Water extract of curcuma longa L. ameliorates non-alcoholic fatty liver disease. *Nutrients*. 2019;11(10):2536. doi:10.3390/nu11102536
12. Ho C, Gao Y, Zheng D, et al. Alisol A attenuates high-fat-diet-induced obesity and metabolic disorders via the AMPK/ACC/SREBP-1c pathway. *J Cell Mol Med*. 2019;23(8):5108–5118. doi:10.1111/jcmm.14380
13. Zhang Q, Jia Y, Zhang Y, et al. The effects of medicinal and food homologous substances on blood lipid and blood glucose levels and liver function in patients with nonalcoholic fatty liver disease: a systematic review of randomized controlled trials. *Lipids Health Dis*. 2023;22(1):137. doi:10.1186/s12944-023-01900-5
14. Chen Z, Li C, Yang C, et al. Lipid regulation effects of raw and processed notoginseng Radix Et Rhizome on steatotic hepatocyte L02 Cell. *Biomed Res Int*. 2016;2016:2919034. doi:10.1155/2016/2919034
15. Ahmad MF, Ahmad FA, Zeyaullah M, et al. Ganoderma lucidum: novel insight into hepatoprotective potential with mechanisms of action. *Nutrients*. 2023;15(8):1874. doi:10.3390/nu15081874
16. Yu LP, Li YQ, Li YJ, et al. In vivo identification of the pharmacodynamic ingredients of Polygonum cuspidatum for remedying the mitochondria to alleviate metabolic dysfunction-associated fatty liver disease. *Biomed Pharmacother*. 2022;156:113849. doi:10.1016/j.biopha.2022.113849
17. Lin Q-H, Liang Q, Shi J-X, et al. Effects of Hujin Decoction on hepatic lipid synthesis in mice with metabolic-associated fatty liver disease through SIRT1/AMPK pathway. *New Chinese Materia Medica Clin Pharmacol*. 2021;32(06):765–770.
18. Huang M. Establishment of Hujinfang fingerprint and its effect on AMPK/mTOR pathway genes in MAFLD mice. Guangzhou University of Chinese Medicine, 2021.
19. Tilg H, Moschen AR. Evolution of inflammation in nonalcoholic fatty liver disease: the multiple parallel hits hypothesis. *Hepatology*. 2010;52 (5):1836–1846. doi:10.1002/hep.24001
20. Mota M, Banini BA, Cazanave SC, et al. Molecular mechanisms of lipotoxicity and glucotoxicity in nonalcoholic fatty liver disease. *Metabolism*. 2016;65(8):1049–1061. doi:10.1016/j.metabol.2016.02.014
21. Qiao HZ, Di LQ, Ping QN, et al. Structural Chinese medicine: new research field on pharmacodynamic substance basis of traditional Chinese medicine]. *Zhongguo Zhong Yao Za Zhi*. 2021;46(10):2443–2448. doi:10.19540/j.cnki.cjcmm.20210129.601
22. Zhao L, Zhang H, Li N, et al. Network pharmacology, a promising approach to reveal the pharmacology mechanism of Chinese medicine formula. *J Ethnopharmacol*. 2023;309:116306. doi:10.1016/j.jep.2023.116306
23. Miao R, Meng Q, Wang C, et al. Bibliometric analysis of network pharmacology in traditional Chinese medicine. *Evid Based Complement Alternat Med*. 2022;2022:1583773. doi:10.1155/2022/1583773
24. Semiserin VA, Karakozov AG, Malkuta MA, et al. Evaluation of the efficiency of hepatoprotective monotherapy using succinic acid and methionine for nonalcoholic fatty liver disease at the stage of steatohepatitis]. *Ter Arkh*. 2016;88(2):58–63. doi:10.17116/terarkh201688258-63
25. Stel'Makh VV, Kozlov VK, Radchenko VG, et al. Pathogenetic therapy of metabolic syndrome at the stage of visceral lesions]. *Klin Med*. 2012;90 (6):61–65.
26. Yang S, Duan Z, Zhang S, et al. Ginsenoside Rh4 improves hepatic lipid metabolism and inflammation in a model of NAFLD by targeting the gut liver axis and modulating the FXR signaling pathway. *Foods*. 2023;12(13):2492.
27. Kim HM, Kim Y, Lee ES, et al. Caffeic acid ameliorates hepatic steatosis and reduces ER stress in high fat diet-induced obese mice by regulating autophagy. *Nutrition*. 2018;55–56:63–70. doi:10.1016/j.nut.2018.03.010
28. Zhang J, Ouyang H, Gu X, et al. Caffeic acid ameliorates metabolic dysfunction-associated steatotic liver disease via alleviating oxidative damage and lipid accumulation in hepatocytes through activating Nrf2 via targeting Keap1. *Free Radic Biol Med*. 2024;224:352–365. doi:10.1016/j.freeradbiomed.2024.08.038
29. Sancheti S, Sancheti S, Seo SY. Ameliorative effects of 7-methylcoumarin and 7-methoxycoumarin against CCl4-induced hepatotoxicity in rats. *Drug Chem Toxicol*. 2013;36(1):42–47. doi:10.3109/01480545.2011.648329
30. Kim YJ, Kim HH, Shin CS, et al. 2'-fucosyllactose and 3-fucosyllactose alleviates interleukin-6-induced barrier dysfunction and dextran sodium sulfate-induced colitis by improving intestinal barrier function and modulating the intestinal microbiome. *Nutrients*. 2023;15(8):1845.
31. Zhang J, Zhang W, Yang L, et al. Phytochemical gallic acid alleviates nonalcoholic fatty liver disease via AMPK-ACC-PPARa axis through dual regulation of lipid metabolism and mitochondrial function. *Phytomedicine*. 2023;109:154589. doi:10.1016/j.phymed.2022.154589
32. Sharma L, Lone NA, Knott RM, et al. Trigonelline prevents high cholesterol and high fat diet induced hepatic lipid accumulation and lipo-toxicity in C57BL/6J mice, via restoration of hepatic autophagy. *Food Chem Toxicol*. 2018;121:283–296. doi:10.1016/j.fct.2018.09.011
33. Li J, Sun Y, Li G, et al. The extraction, determination, and bioactivity of curcumenol: a comprehensive review. *Molecules*. 2024;29(3):656.
34. Li G, Xie H, Cao X, et al. Ginsenoside Rg1 exerts anti-apoptotic effects on non-alcoholic fatty liver cells by downregulating the expression of SGPL1. *Mol Med Rep*. 2022;25(5). doi:10.3892/mmr.2022.12694

35. Li M, Xiao Y, Xiao L, et al. Epigoitrin alleviates lipid and glucose metabolic disorders induced by a high-fat diet. *Food Funct*. 2022;13 (13):7260–7273. doi:10.1039/D2FO00242F
36. Tanase DM, Gosav EM, Costea CF, et al. The intricate relationship between type 2 diabetes mellitus (T2DM), insulin resistance (IR), and nonalcoholic fatty liver disease (NAFLD). *J Diabetes Res*. 2020;2020:3920196. doi:10.1155/2020/3920196
37. Zhuang S, Zhou X, Yang X, et al. Dendrobium mixture ameliorates hepatic injury induced by insulin resistance in vitro and in vivo through the downregulation of AGE/RAGE/Akt signaling pathway. *Heliyon*. 2023;9(11):e22007. doi:10.1016/j.heliyon.2023.e22007
38. Asadipooya K, Lankarani KB, Raj R, et al. RAGE is a potential cause of onset and progression of nonalcoholic fatty liver disease. *Int J Endocrinol*. 2019;2019:2151302. doi:10.1155/2019/2151302
39. Li CP, Li JH, He SY, et al. Roles of Fas/Fasl, Bcl-2/Bax, and Caspase-8 in rat nonalcoholic fatty liver disease pathogenesis. *Genet Mol Res*. 2014;13 (2):3991–3999. doi:10.4238/2014.May.23.10
40. Keating SE, Chawla Y, De A, et al. Lifestyle intervention for metabolic dysfunction-associated fatty liver disease: a 24-h integrated behavior perspective. *Hepatol Int*. 2024;18(Suppl 2):959–976. doi:10.1007/s12072-024-10663-9
41. Song Y, Ni W, Zheng M, et al. Vitamin E (300 mg) in the treatment of MASH: a multi-center, randomized, double-blind, placebo-controlled study. *Cell Rep Med*. 2025;6(2):101939. doi:10.1016/j.xcrm.2025.101939
42. Abdel MM, Adel A, Abbassi MM, et al. Efficacy and safety of dapagliflozin compared to pioglitazone in diabetic and non-diabetic patients with non-alcoholic steatohepatitis: a randomized clinical trial. *Clin Res Hepatol Gastroenterol*. 2025;49(3):102543. doi:10.1016/j.clinre.2025.102543
43. Wu WK, Chen YH, Lee PC, et al. Mining gut microbiota from bariatric surgery for MAFLD. *Front Endocrinol*. 2021;12:612946. doi:10.3389/fendo.2021.612946